Efficiency of Charge Transport in a Polypeptide Chain: The Isolated System

Sheh-Yi Sheu,[†] E. W. Schlag,*[,‡] Dah-Yen Yang,[§] and H. L. Selzle[‡]

Department of Life Science, National Yang-Ming University, Taipei 112, Taiwan, Institute fuer Physikalische und Theoretische Chemie, Technische Universitaet Muenchen, Lichtenbergstrasse 4, D-85748 Garching, Germany, and Institute of Atomic and Molecular Science, Academia Sinica, Taipei 106, Taiwan

Received: February 15, 2001; In Final Form: April 16, 2001

We employ new single site molecular dynamics calculations to determine the time development of initial energization at an excitation site moving to a terminus. For this we find the efficiency of charge transport in an isolated polypeptide. Based on our bifunctional model (Schlag, E. W.; Sheu, S.-Y.; Yang, D.-Y.; Selzle, H. L.; Lin, S. H. *Proc. Natl. Acad. Sci. U.S.A.* **2000**, *97*, 1068), the charge transport along a polypeptide chain involves essential large amplitude chain motions and can be depicted as a virtual particle moving inside the bottom of a Ramachandran plot. The polypeptide is locally excited at a specific residue (or local heating), from which the energy is propagated. The motion of the virtual particle approaches a ballistic behavior. Energy conservation is observed, which ensures, at long distance, movement of the charge and energy and hence provides a model for chemical reaction at a distance. The high efficiency of charge transport is preserved down the chain in agreement with the experiment. Peptides thus represent a new unique class of molecular systems with near ideal conduction in the isolated state—the task remains to define a suitable environment to maintain this high conductance.

I. Introduction

Recently, the charge transport process in DNA and proteins over long distances has attracted considerable attention.[1−10] This is a fundamental important process in biological systems, and since reactive chemistry at long distance from the site of initiation is often connected to such transport, it can also be denoted as a distal reactivity.[11−14] It is of some import to understand the mechanism for reaction at a distance, particularly in biological systems.

Isied et al.[15−17] studied a short polypeptide mediated charge transport system dissolved in water. The charge transport process in a real protein has been investigated experimentally for α-helix (myoglobin) and β-sheet (azurine).[18,19] In Gray's experiments, the protein is dissolved in water. In the solvent the β-sheet has a higher efficiency than the α-helix. The efficiency of charge transport along a real protein dissolved in a solvent is described by a β value based on an exponential decay in a network theory of a nonadiabatic ET rate without any explicit protein dynamic effects being included.[20] The protein interestingly shows a very much higher charge transport efficiency as an isolated molecule in the gas phase, the loss in water we attribute here, on the basis of our model calculations, to a water barrel effect.

It is important to understand the intrinsic property of charge transport in a pure polypeptide chain before we proceed to the solvent dynamic effect. In the gas phase, Schlag and co-workers[21−26] found a very high efficiency for charge transport in polypeptides. To understand these results, a bifunctional model has been proposed by Schlag et al.[27,28] involving charge transport in a polypeptide chain at room temperature. This model shows a fast electronic charge transport rate combined with specific dynamic effects. A protein dynamic effect is not included in typical network theory although, in general, dynamic effects on charge transport are known[29] and have been recently invoked for DNA.[30−32]

Along a polypeptide chain, at each C_α-atom, the torsional angles ϕ and ψ are constrained within a certain region and, as defined in a Ramachandran plot, near that of an α-helix or a β-sheet. Such motion is particularly important when the secondary structure of a protein is generated, which we find occurs for a protein chain residue number larger than 5. Our bifunctional model shows that the motion of the torsional angles ϕ and ψ can be mapped into a virtual Brownian particle moving essentially without a barrier inside the Ramachandran plot with an exit gate; this barrierless trough defines the BS box.[28] In this exit gate the charge is transferred as dictated by the electronic states of the residues. Hence the dynamic behavior of charge transport in a polypeptide chain is described by a sequential jumping between several connected BS boxes.[28]

A global heating molecular dynamic simulation of a short polypeptide chain displays a stochastic behavior for the virtual particle motion inside the BS box. The first passage time distribution of the escape process in the BS box, though, including near zero phonon modes, is in good agreement with mean first passage time of the charge transport process in a polypeptide chain calculated in molecular dynamics.

In this paper, we push our bifunctional model further and introduce a new single site version of a MD program to follow excitation from a fixed location and thus directly explain the high efficiency observed by Schlag and co-workers for charge transport in polypeptides in the gas phase.[23] In their experiment, the charge is excited at the C-terminal of the polypeptide chain and is propagated to the N-terminal of the polypeptide chain without any bond breaking at any intermediate residues. Since the experiment is performed in a cooled jet at some 50−100 K, the polypeptide chain configuration is quite rigid and the

* Corresponding author. Fax +49 89 289 13389. E-mail: schlag@ch.tum.de.
[†] National Yang-Ming University.
[‡] Technische Universitaet Muenchen.
[§] Academia Sinica.

10.1021/jp010603c CCC: $20.00
Published on Web 06/07/2001

degrees of freedom involved in a low-temperature regime and short time regime are few. We argue that the vibrational modes are not yet in action due to temperature and the short inter-residue transition time. Only the motion of the ϕ and ψ torsional angles is involved. Hence the motion in the BS box is nearly ballistic. This ballistic behavior can here now be directly supported by MD calculations.

II. Review of Bifunctional Model

There are some 22 different kinds of natural amino acids found in a protein. The charge transfer between amino acids is at the C_α-atom. Each C_α-atom has a N-side and a C-side. The torsional angles around the C_α-hinge are confined within a certain domain inside the configuration space (ψ, ϕ), which is called the Ramachandran plot. Different subregions inside the Ramachandran plot are for the α-helix and the β-sheet. In other words, for these features the residue number of the polypeptide chain should be at least larger than 5. However, since the potential surfaces defined by the allowed ϕ and ψ angles are nearly square wells, even for a short polypeptide chain, the torsional angles around the C_α-hinge are also confined to certain subregions inside the Ramachandran plot. When the charge is locally excited at the C-side of one C_α-atom, it propagates or jumps between connected amino acids through O−O-atom "collision" of adjacent carbonyl groups around the C_α-hinge. Hence the rotational motion of the carbonyl group along the $C_\alpha N$ and $C_\alpha C$ axes of the C_α-hinge dominates the dynamics of the charge transport process. The vibrational modes are considered not active on such a short time (150 fs) scale. The rotational motion of these torsional angles corresponds to a virtual particle moving inside the Ramachandran plot with certain contact angles for O−O-atoms where charge is transported. This subregion with a contact region or gate part is referred to as the BS box.

III. Molecular Dynamic Simulation Method: Local Heating

In our bifunctional model, the charge is transported along a polypeptide chain. At each C_α-atom, the torsional angles ψ and ϕ are constrained in the Ramachandran plot (see Figure 1A). The $\overrightarrow{C_\alpha N}$ and $\overrightarrow{C_\alpha C}$ of the C_α-atom form a hinge. The charge is transported from the C-side of the C_α-atom to the N-side. Before the charge is transported, it waits in the C−side until the O−O-atoms between two connected amino acids collide. The rotational motion of the ψ and ϕ angles is similar to a Brownian particle moving inside a 2D box with a static gate where the O−O-atoms collide with each other and charge starts to transfer.

In our previous work,[27−28] we studied the escape time of the Brownian particle inside a 2D finite box with a gate. Meanwhile, we demonstrated the concept of the BS box with extensive MD calculations and also simulate the first passage time (fpt) distribution of a $(Gly)_n$ polypeptide chain at 2000 K, i.e., a global heating procedure. This thermal energy corresponds just to the local charge energy. In our original global MD simulation work, we allowed the entire small polypeptide chain to move randomly at 2000 K and hence many of the phonon modes are pumped up, i.e., a large scale fluctuation.

In the present paper we introduce a substantial modification to the conventional MD programs, which now comes closer to the real case employing a local heating method. It now uniquely defines the site of initiation as is the case in many biological processes. Such site identification has very general applications to MD simulations and is of particular importance for studying the early history of the evolution of a system. This shows that

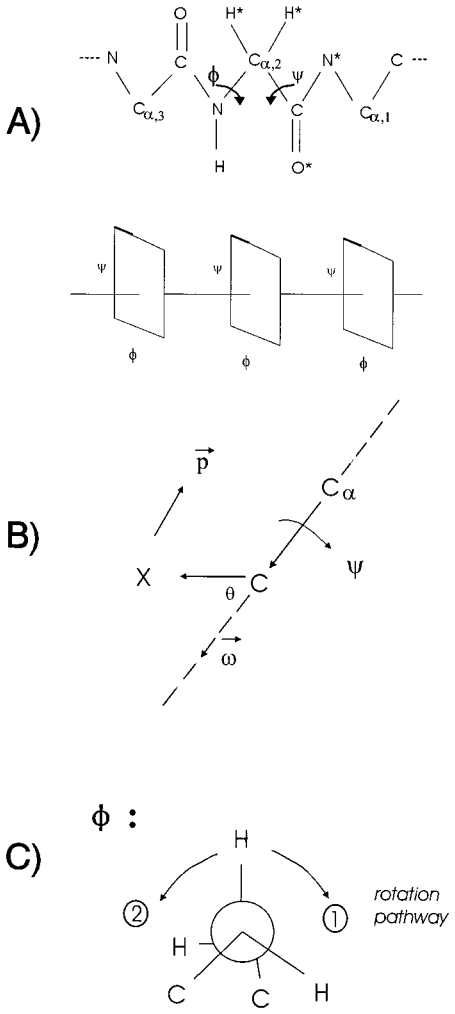

Figure 1. Scheme for bifunctional model. (A) Sequential hopping between residues. At each C_α-atom, there is a pair of torsional angles ψ and ϕ. These define the so-called C_α-hinge. Below the polypeptide chain, we show the corresponding BS box with a gate (bold line). The star on the atom indicates the locally heated atom. (B) Local heating procedure. Here we define the vectors $\vec{\omega}$ and $\vec{p}$. (C) Rotation pathway. Before the charge is transported, it waits in the C-side of the C_α-hinge. Our local heating procedure enhances the rotation frequency in any of the rotation pathways.

not only were the extra phonon modes created in the global heating simulation result but now these can be removed. More importantly, the Brownian motion inside the BS box idea is now kept intact. These single site local heating results are now interestingly in complete agreement with our prior global method limited to short times. This more sophisticated local heating method now extends our previous work to more realistic protein systems and even makes the solvated protein system simulation now possible. In the present paper, we will define this single site local heating method and obtain the first passage time distribution, which displays the absence of the extra phonon modes. The efficiency of a successful collision is then related to the β value and the activation energy of the charge transport process.

Let us consider how to heat up the rotational mode of the ψ-angle on the C−side of the C_α-hinge. We define the $\overrightarrow{C_\alpha C}$ and $\overrightarrow{CX}$ vectors from C_α-atom to C-atom and from C-atom to X-atom, respectively. Here X-atom can be any atoms bonded to the C-atom (see Figure 1A). The vector orthogonal to the $\overrightarrow{C_\alpha C}$ axis is defined by $\overrightarrow{CX}_\perp = \overrightarrow{CX} \times \sin\theta$, where $\cos\theta = \overrightarrow{C_\alpha C}\cdot\overrightarrow{CX}/|\overrightarrow{C_\alpha C}| \times |\overrightarrow{CX}|$. There are two unknown vectors that

need to be solved (see Figure 1B). The first one is the torsional angular momentum. We set its rotation axis along the $\overrightarrow{C_\alpha C}$ vector by $\vec{\omega} = \overrightarrow{C_\alpha C}/|\overrightarrow{C_\alpha C}| \times \omega$, where we provide a rotation energy $^1/_2 I\omega^2$ (in units of thermal energy) to the X-atom (I is the inertial moment). Hence, we have the relationship of $\overrightarrow{CX}_\perp \times \vec{p} = \vec{\omega}$. Second, the excited angular velocity of the X-atom, $\vec{p}$, should be tangential. We find that $\vec{p}/|\vec{p}| = \overrightarrow{CX}_\perp \times \overrightarrow{C_\alpha C}/|\overrightarrow{CX}_\perp| \cdot |\overrightarrow{C_\alpha C}|$ and the magnitude of $\vec{p}$ is $\omega \times |\overrightarrow{CX}_\perp| \times (\overrightarrow{CX}_\perp \times \overrightarrow{C_\alpha C})/|\overrightarrow{CX}_\perp| \cdot |\overrightarrow{C_\alpha C}|^{-1}$. Here the unit of ω is changed into MD velocity. In our MD simulation, we provide a charge energy ($E = {}^1/_2 I\omega^2$), which is ca. E_{1667K}, to the atoms attached to the ψ axis, i.e., N-, O-, and H-atoms. Here the charge energy or excitation energy E is in units of thermal energy. The rest of the atoms in the polypeptide chain are still kept at 300 K as the background temperature. Typically, in each simulation, 3000 configurations have been chosen. Only part of the configurations have a successful O−O collision, i.e., O- and O-atoms come close to a certain distance, e.g., 2.8 Å. Hence we now define the efficiency as

$$\text{efficiency} = \text{successful configurations/total configurations} \quad (1)$$

In our simulation, a single site modified CHARMM 24 program[33] is introduced, implementing the local heating method described in preceding paragraphs. Three different kinds of rotational direction (see Figure 1C) have been chosen such as positive (pathway 1), negative (pathway 2), and mixed (or random, pathway 1 + 2) rotation around the ϕ-angle. For random initial "trans" configuration of O−O-atoms, the direction of rotation does not show any differences. However, for the native initial configuration, the rotational direction or pathway directly affects the mean free path or mean free time.[7] The mean free time is reflected as the peak position of the fpt curve.

We employ instantaneous heating procedures for the single site that is ca. 3 fs or only three molecular dynamic steps. Energy is transferred along the polypeptide chain down to the next nearby C_α-hinge.

The virtual particle motion inside the BS box is shown to follow a stochastic process. Our earlier global heating method revealed a large scale fluctuation of the polypeptide chain and a vast amount of vibrational modes being excited. Interestingly, the newly developed single site local heating method effectively suppresses the vibrational modes but fully keeps the rotational pathways of the escape process. The time is simply too short to produce any substantial vibrational excitation. The first passage time distribution of the O−O-atoms collision is a combination of escape process and internal rotational motion at high temperature. The mean first passage time for the O−O-atoms to collide is $\tau = \sqrt{2} \cdot 2\pi/\theta$ and is obtained by solving the 2D Smoluchowski equation with a radiation boundary condition. The gate part is situated at the perimeter of the 2D disk and is expressed by the ratio of the gate to the total perimeter length. Here θ is the maximum gate-opening angle. In the high-temperature regime, the vibrational motion sets in and the rotational energy is dissipated very fast. The efficiency is defined as the ratio of successful runs to the total configurations. The distance decay factor β value can be expressed in terms of the efficiency as $\beta = -\ \ln(\text{efficiency})/3.7$, where the typical interresidue spacing is taken to be 3.7 Å. A local heating MD simulation result shows that a high efficiency is obtained at five residues away from the excited residue at 300 K. This shows energy being transferred before it is dissipated.

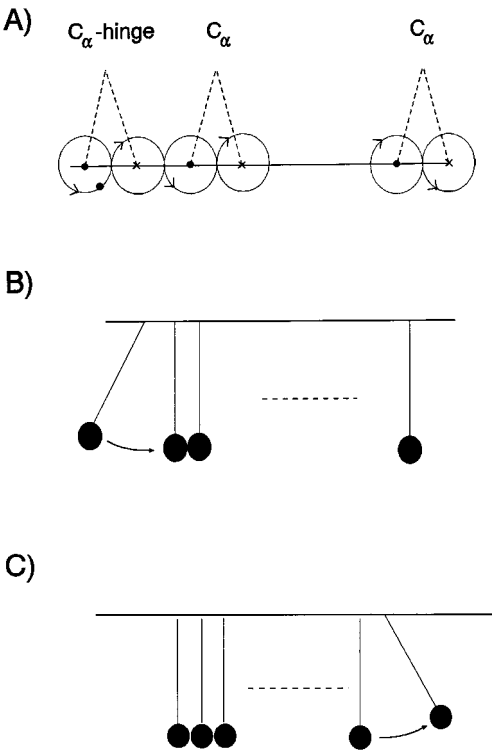

Figure 2. Energy transfer scheme in bifunctional model. (A) Dashed lines correspond to the $C_\alpha C$ and $C_\alpha N$ rotational axes. Before the vibrational mode sets in, the circle and the dot on it represent the rotational motion of the O-atom on the carbonyl group. The excited carbonyl group on the C-side of the C_α-hinge moves along the circle and hit the other O-atom on the N-side of the carbonyl group and so on. (B) The big black circle corresponds to an O-atom on the carbonyl group, and the system (or polypeptide chain) is excited from the left-hand side (C-terminal). (C) Energy is transferred from left-hand side (C-terminal) to the right-hand side (N-terminal). The black circle can be understood as a hard sphere.

IV. Results and Discussion

A study of the mass spectrum of small polypeptide chains $(Leu)_n Trp$ ($n = 1-4$) shows only parent ion and N-terminals with total efficiency ca. 0.47.[34] There is no other bond breaking at the intermediate residues. Hence the efficiency is 0.47 for the first residue and other residues have unit efficiency. This unit efficiency guarantees that the energy is transferred perfectly. In the gas phase experiment, the charge excitation energy drives the rotational mode of the torsional angles around the C_α-atom before the vibrational modes set in. This is a basic mechanism in our bifunctional model. However, the energy flow problem could not be addressed in conventional MD calculations and hence was not included in our previous work. By use of the local heating method, the remaining phonons are seen not to influence the subsequent motion leading to the charge transport process. Hence the energy is essentially not dissipated. The results confirm a near unit efficiency and a ballistic motion (in the sense of the energy conservation) in the bifunctional model. To illustrate the energy conservation in the energy transfer process in our bifunctional model, we can explain the energy conservation with a simple mechanical bead model. The rotational motion of the carbonyl groups around the ϕ and ψ angles is portrayed in Figure 2A. The motion of the carbonyl group in the local heating process (or forced motion) is similar to a bead moving along a circular orbit and the sequence of the circular orbit connected at the contact point only. Once the first bead is locally excited, for example, the bead on the first circular orbit rotates to collide with the second bead at the contact point.

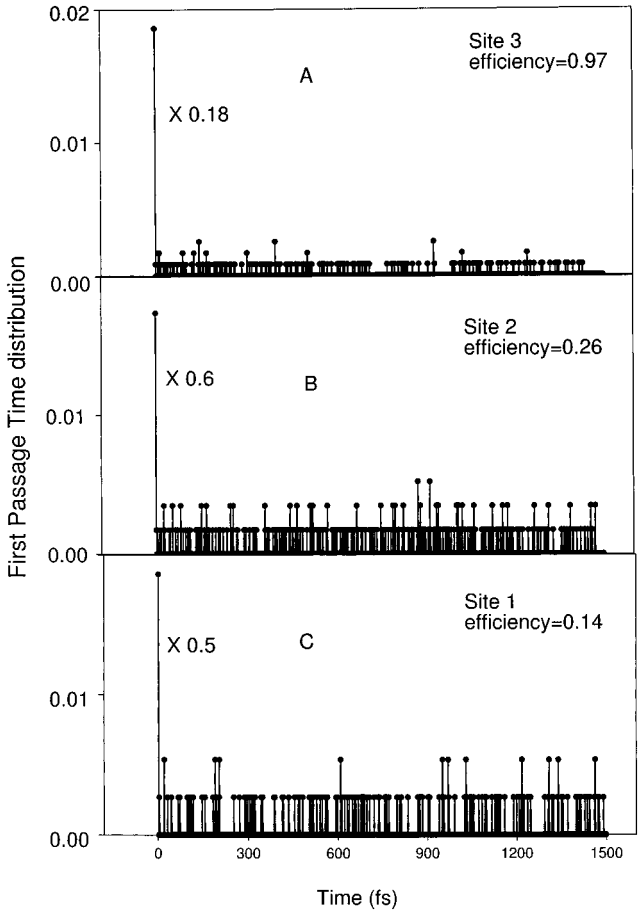

Figure 3. Flexible system first passage time distribution vs time. The initial structure of the short Ala−Ala_1−Ala_2−Tyr_3 polypeptide chain is obtained by energy minimization. The local heating site is Tyr_3 with excitation energy 1667 K. The background temperature is 50 K.

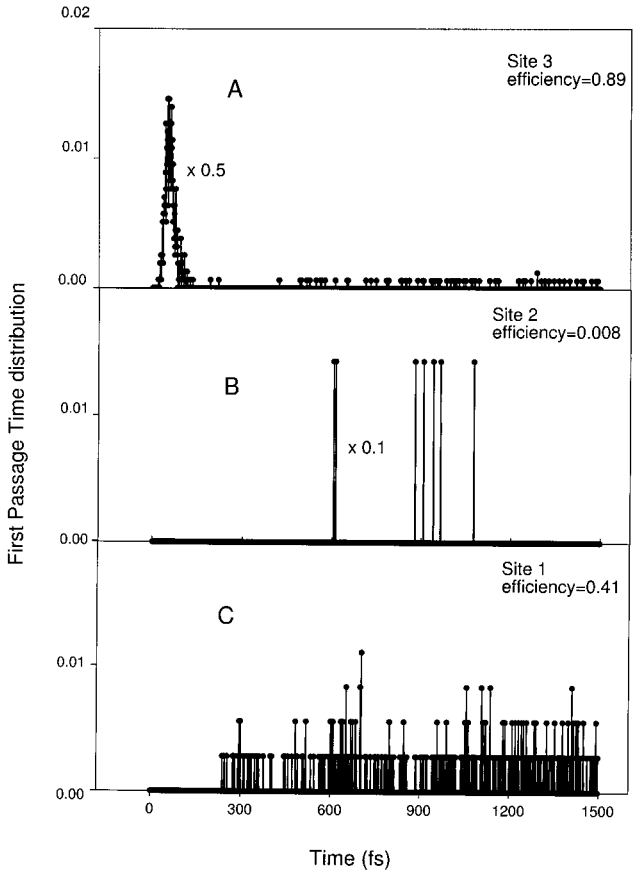

Figure 4. Rigid system first passage time distribution vs time. The Ala_1−Ala_2 methyl groups of the short Ala−Ala_1−Ala_2−Tyr_3 polypeptide chain are bonded to form a six-member ring. The O−O-atoms at Ala_1 and Ala_2 never collide. Since we normalized the fpt curve with the successful O−O collision, in (B) the relative peak is high but the efficiency is very small.

Because of the energy conservation (or momentum conservation for a hard bead) law, for equal mass beads, the total energy of the first bead maybe transferred to the second bead. Hence, the total energy can be transferred to the last bead. A similar energy transfer process for hard beads is depicted in Figure 2B,C. The energy transfer is conserved.

The efficiency for this ballistic model can be explained in the following way. Assume for a linear polypeptide chain with n residues, the nearest-neighbor charge-transfer probabilities from the ith C_α-atom at time t are $\Psi_{i+1,i}(t)$ and $\Psi_{i-1,i}(t)$. This transition probability should satisfy the following conservation relationships for the waiting time distribution $\Psi_i(t)$:

$$\Psi_i(t) = \Psi_{i+1,i}(t) + \Psi_{i-1,i}(t) \tag{2}$$

and the normalization condition

$$\int_0^\infty \mathrm{d}t\, \Psi_i(t) = 1 \tag{3}$$

The total probability at time t from C-terminal to N-terminal is

$$\Psi_{\mathrm{N,C}}(t) = \prod_{i=0(\text{C-terminal})}^{n-1(\text{N-terminal})} \Psi_{i+1,i}(t) \tag{4}$$

The ballistic model is actually a no-back-reaction case, i.e., $\Psi_{i-1,i}(t) = 0$. Hence all of the forward transition probability is 1 and the total efficiency is unity.

To have a clear example of our transport process, we performed calculations on a model short polypeptide chain such as Ala−Ala_1−Ala_2−Tyr_3. The subscript here means the O−O pair in the short polypeptide chain. The local heating site is at Tyr_3 (i.e., a C-terminal). Here we heat up the benzene ring, C-, O-, and H-atoms in Tyr_3 with excitation energy 1667 K. The initial structure of the Ala−Ala_1−Ala_2−Tyr_3 chain is energy minimized (structure I) and the background temperature is kept at 50 K for a suitable condition of mass spectroscopy. For this loose system in Figure 3A, the efficiency at starting site 3 is close to unity and the first peak of the fpt distribution curve located at 1 fs is very sharp. The first peaks at the further sites in Figure 3B,C decrease their intensity and the efficiency at site 1 is ca. 0.14. Now we inhibit the BS motion by binding the methyl groups between Ala_1−Ala_2 to make a local six-member ring (structure II). Since in this structure II the O−O-atom motion is restricted, the ψ and ϕ angles rotations are limited due to the ring; hence charge is not transported down the polypeptide chain. Figure 4A at the start displays a sharp peak at 5 fs and the efficiency is close to 1. Note in particular that the first peak distribution is different from that in Figure 3A. This is due to the energy flow being modified by the ring. Now, for this rigid structure in Figure 4B, at site 2 no peak shows up and the efficiency for a O−O collision is close to zero. Hence no charge transport. However, at the final site in Figure 4C the efficiency is close to 0.41 and there is no sharp peak located around 5 fs. Although there is now energy present for the BS motion, it is of no avail since no charge is arriving from the prior site. Hence there is no charge flowing down the chain to

TABLE 1: Efficiency at Each Site Away from the Local Heating Site[a]

residue no.	efficiency
2	0.22
3	0.0048
4	0.47
5	0.34
6	0.41
7	0.58
8	0.93
9	1.0
10	0.895
11	0.83
12	0.70
13	0.29
14	0.12
15	0.14
16	0.049
17	0.069
18	0.011
19	0.021
20	0.256

[a] Local heating site = Thr_9. Local heating temperature = 1667 K. Background temperature = 300 K. O−O distance = 2.8 A. •Mb_{20} = (N-terminal)Glu_1−Asp_2-Leu_3-$Lysn_4$-$Lysn_5$-Hsd_6-Gly_7−Val_8−Thr_9−Val_{10}-Leu_{11}−Thr_{12}-Ala_{13}−Leu_{14}-Gly_{15}−Ala_{16}−Ile_{17}-Leu_{18}-$Lysn_{19}$-$Lysn_{20}$(C-terminal).

TABLE 2: Efficiency at Each Site Away from the Local Heating Site[a]

residue no.	efficiency
2	0.15
3	0.001
4	0.34
5	0.24
6	0.24
7	0.34
8	0.62
9	0.83
10	1.0
11	0.76
12	0.89
13	0.41
14	0.22
15	0.22
16	0.066
17	0.070
18	0.0097
19	0.013
20	0.20

[a] Local heating site = Val_{10}. Local heating temperature = 1667 K. Background temperature = 300 K. •Mb_{20} = (N-terminal)Glu_1−Asp_2-Leu_3-$Lysn_4$-$Lysn_5$−Hsd_6-Gly_7−Val_8−Thr_9−Val_{10}-Leu_{11}−Thr_1-Ala_{13}−Leu_{14}-Gly_{15}−Ala_{16}−Ile_{17}-Leu_{18}-$Lysn_{19}$-$Lysn_{20}$(C-terminal).

site Ala for structure II. The fpt curve in Figure 4C just shows a thermal distribution. This means that the rigid structure II has less energy dissipation than the loose structure I, so that more energy arrives at the final site (Ala), in turn producing more O−O collisions but not producing more charge flow, since there is a severe charge blockage at site 2, as seen in Figure 4B. So what charge is not at site 2 in Figure 4B cannot arrive at site 1 in Figure 4C. On the other hand, the energy at site 3 does arrive at site 1, in fact, even better than for the structure I.

We next turn to study the energy flow down the real protein chain, we pick a small polypeptide chain cut from a myoglobin crystal structure with 20 amino acids. The small polypeptide chain Mb_{20} structure is minimized first. This is the initial configuration of our local heating simulation. The single site local heating excitation energy is ca. 150 meV (=1667 K) and the polypeptide chain background temperature is ca. 300 K. To observe the energy flow, the polypeptide chain temperature is not renormalized. We study the energy flow down the chain from the C-side of the C_α-atom to its N-side by examining the first passage time distribution. Meanwhile, the high efficiency of the successful O−O collision at each residue after local heating is observed.

In Table 1 and 2, we list the efficiency at each site. The polypeptide chain background temperature is 300 K. Comparing Tables 1 and 2, though we locally heat the single site Thr_9 in Table 1 and Val_{10} in Table 2, the efficiency drops until the fourth site away from the local heating site. Hence the efficiency drop is independent of the type of residue. In Table 3, we show the temperature effect of the efficiency. The local heating site is at

TABLE 3: Efficiency at Each Site Away from the Local Heating Site[a]

residue no.	efficiency
2	0.18
3	0.0033
4	0.41
5	0.29
6	0.25
7	0.40
8	0.69
9	0.85
10	1.0
11	0.78
12	0.90
13	0.46
14	0.22
15	0.22
16	0.084
17	0.11
18	0.013
19	0.025
20	0.26

[a] Local heating temperature = 2667 K. Background temperature = 300 K. •Mb_{20} = (N-terminal)Glu_1−Asp_2-Leu_3-$Lysn_4$-$Lysn_5$-Hsd_6-Gly_7−Val_8−Thr_9−Val_{10}-Leu_{11}−Thr_{12}-Ala_{13}−Leu_{14}-Gly_{15}−Ala_{16}−Ile_{17}-Leu_{18}-$Lysn_{19}$-$Lysn_{20}$(C-terminal).

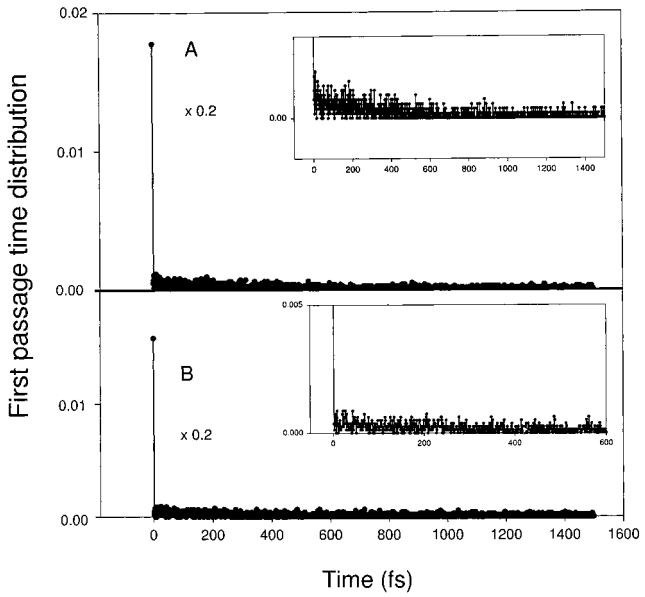

Figure 5. First passage time distribution vs time. The entire Mb_{20} α-helix is globally heated at 1667 K. This is the same as an escape process for a virtual Brownian particle inside the BS box. Since the entire Mb_{20} chain has the same temperature and no energy flows along the chain, there is no structure in the fpt curve. The fpt curve approaches a nonzero value at long time. Here (A) is for the Thr_9 site, and (B), for the Val_{10} site.

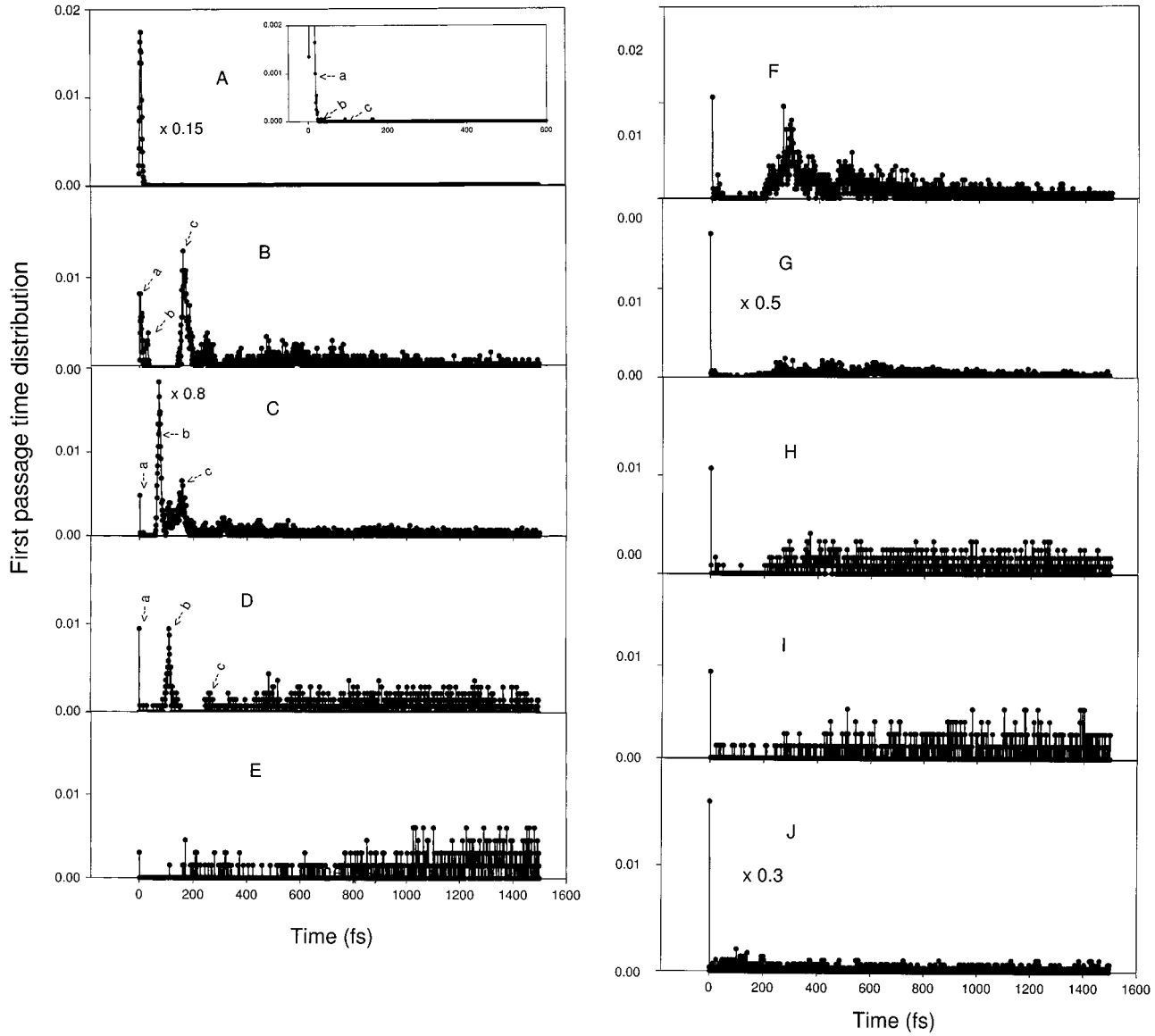

Figure 6. First passage time distribution vs time. The excitation energy is ca. 2667 K, and the local heating site is at Val_{10}. The background temperature is 300 K. At the initial stage, there are three peaks generated in figure (A). Peak a denotes the rotational motion of the C-side carbonyl group directly hits the N-side carbonyl group starting from the native structure of Mb_{20}. Peak b corresponds to a short wandering in the initial direction of the C-side carbonyl group. Peak c shows a random motion of the C-side carbonyl group inside the BS box. The distribution in the peak c part is similar to a thermal distribution. The figures (B)−(E) express the propagation of the peaks to the right. This peak propagation shows an energy transfer along the polypeptide chain. The efficiency drops at Leu_{14} (or E). The propagation from the C-side to the N-side in (F)−(J) also shows a similar energy flow. The figures correspond to Val_{10} (A), Leu_{11} (B), Thr_{12} (C), Ala_{13} (D), Leu_{14} (E), Thr_9 (F), Val_8 (G), Gly_7 (H), Hsd_6 (I), and $Lysn_5$ (J).

Val_{10}, and the background temperature is 300 K. The efficiency increases when the local heating temperature is increased to 2667 K. Since the background temperature is room temperature, the efficiency increase is not so high. But the trends of the efficiency increasing supports the argument that with high local heating energy the efficiency in general will approach unity.

In Figure 5, we show the global heating result of the fpt distribution of Mb_{20} with $T = 1667$ K. Since the initial configuration is the α-helix structure of Mb_{20}, the O−O distance is short and their collision occurs at very short time. This fpt distribution is displayed for the escape process at the Thr_9 and the Val_{10} residue and the long-time tail approaches a thermal noise, as we observed in ref 27. Interestingly, the fpt distribution shows no difference for different residues.

In Figure 6, we excite the C-side of the C_α-hinge at the Val_{10} site with excitation energy 2667 K. The efficiency is estimated from beginning to 1500 fs. Its value is close to unity even at the fourth site away from the local heating site. At the fourth site Leu_{14}, the efficiency decreases abruptly. When we check the first passage time distribution curve in Figure 6A, the first peak (a) is extremely high. This peak is situated at 1 fs right after the C-side of the C_α-hinge is excited. This confirms the ballistic motion of the carbonyl group that moves directly toward the carbonyl group on the N-side of the C_α-hinge. The second peak (b) that occurs at 3 fs is due to the initial random distribution of the "trans" configurations. The third peak (c) situated at 310 fs is due to the random motion of the carbonyl group and the rotational energy is dissipated to vibrational modes or thermal motion. This certainly demonstrates that at the local heating site the energy is mainly kept in the rotational degrees of freedom (peak a) and a very small ratio of the energy is dissipated (peak c).

At the site Leu_{11} next to the local heating site, the efficiency is unity and the first peak (a) in Figure 6B is lowered. However,

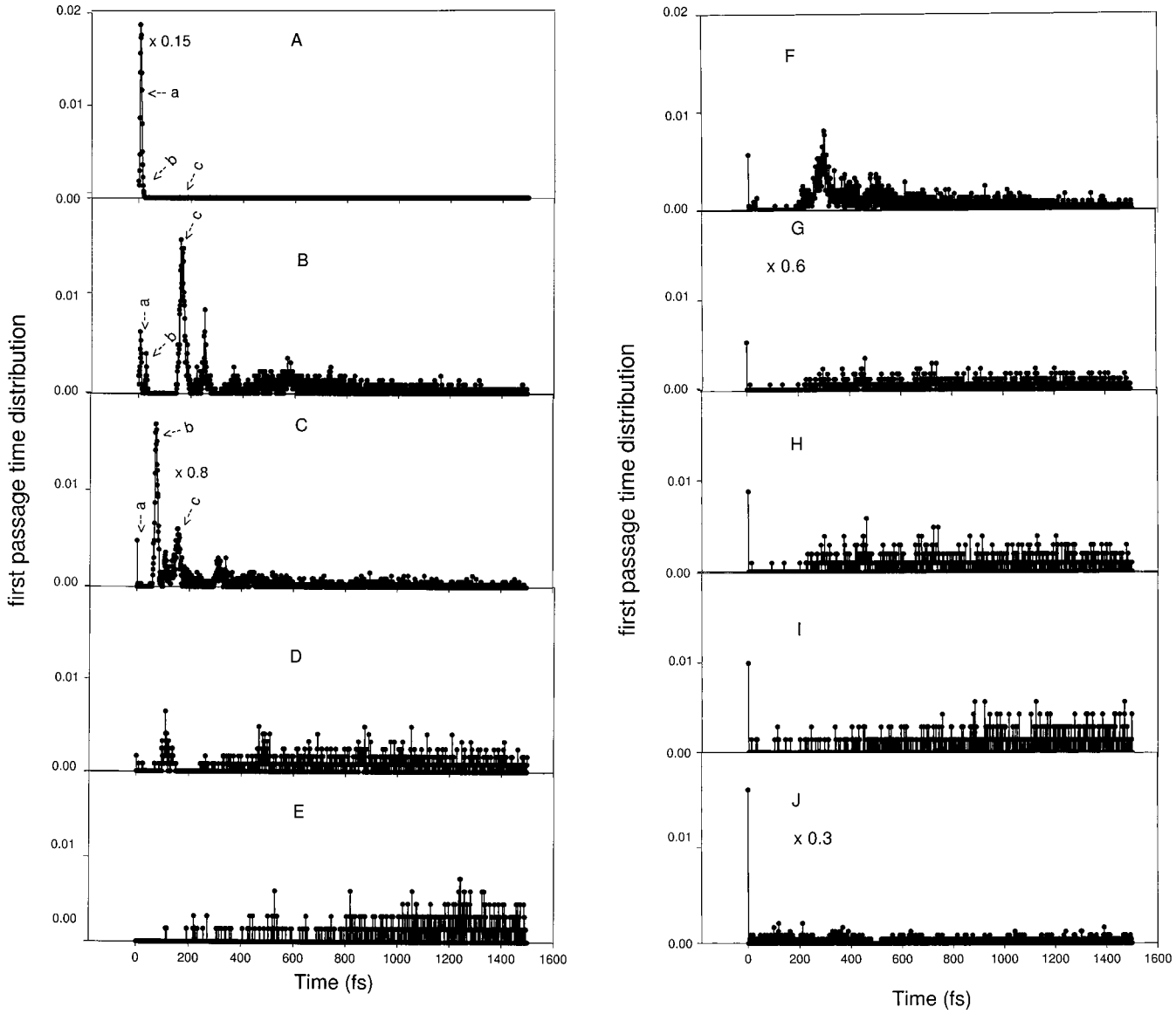

Figure 7. First passage time distribution vs time. The excitation energy is ca. 1667 K, and the local heating site is at Val_{10}. The background temperature is 300 K. Peaks a−c also show up, as compared to Figure 6, but with a lower intensity due to the temperature effect. The figures correspond to Val_{10} (A), Leu_{11} (B), Thr_{12} (C), Ala_{13} (D), Leu_{14} (E), Thr_9 (F), Val_8 (G), Gly_7 (H), Hsd_6 (I), and $Lysn_5$ (J).

the second peak (b) and the third peak (c) are shifted to the right. These peaks are also broadened due to the random motion. In particular, peak c is broadened and is similar to a Gaussian distribution. This ensures that peak c corresponds to a stochastical motion inside the BS box. In the Figure 6C,D, the peaks are broadened and shifted to the right. At the fourth site, in Figure 6E, the efficiency changes abruptly and peak c almost disappears.

Now we decrease the excitation energy from 2667 to 1667 K in Figure 7. Peaks a−c all show up. However, the peaks shifted rate in Figure 7 is similar to that Figure 6. Only the efficiency is decreased. Moreover, the efficiency drops also at the fourth site. The energy flow time is about 3 ps. This is the energy dissipation time scale. In other words, the excitation energy is dissipated at the fourth site away from the local heating site.

In Figure 8, we examine the site effect. The local heating site is at Thr_9. The excitation energy is 2667 K, and the polypeptide chain background temperature is 300 K. The efficiency drops at the fourth site, and this is independent of the kind of the residue. The energy dissipation only depends on the site number.

Now we turn to discuss the efficiency for the entire polypeptide chain. In Table 4, the local heating site is at the C-side of $Lysn_{20}$ with an excitation energy of 1667 K. The efficiency for the local heating site is close to unity and for the N-terminal is still about 0.21. However, due to the large side chain attached to the C_α-atom of Leu, when the amino acid Leu is far away from the local heating site, the corresponding efficiency is relatively small. Due to the heavy weight of the side chain, the motion in its corresponding BS box is slow (see Leu_3 and Leu_{18} in Tables 1−3 and Leu_3, Leu_{11}, and Leu_{14} in Table 4). Moreover, even for the long polypeptide chain the conclusions of $(Leu)_n$Trp and $Ala-Ala_1-Ala_2-Tyr_3$ confirm our model in Figure 2.

In our bifunctional model, the local heating energy or laser pump energy is large enough to drive the charge transport from the C-side of the C_α-atom to its N-side. The fpt curve shows fine structures that correspond to the energy flow during the charge transport. The efficiency changes abruptly at the fourth site away from the local heating site. This is just the time scale

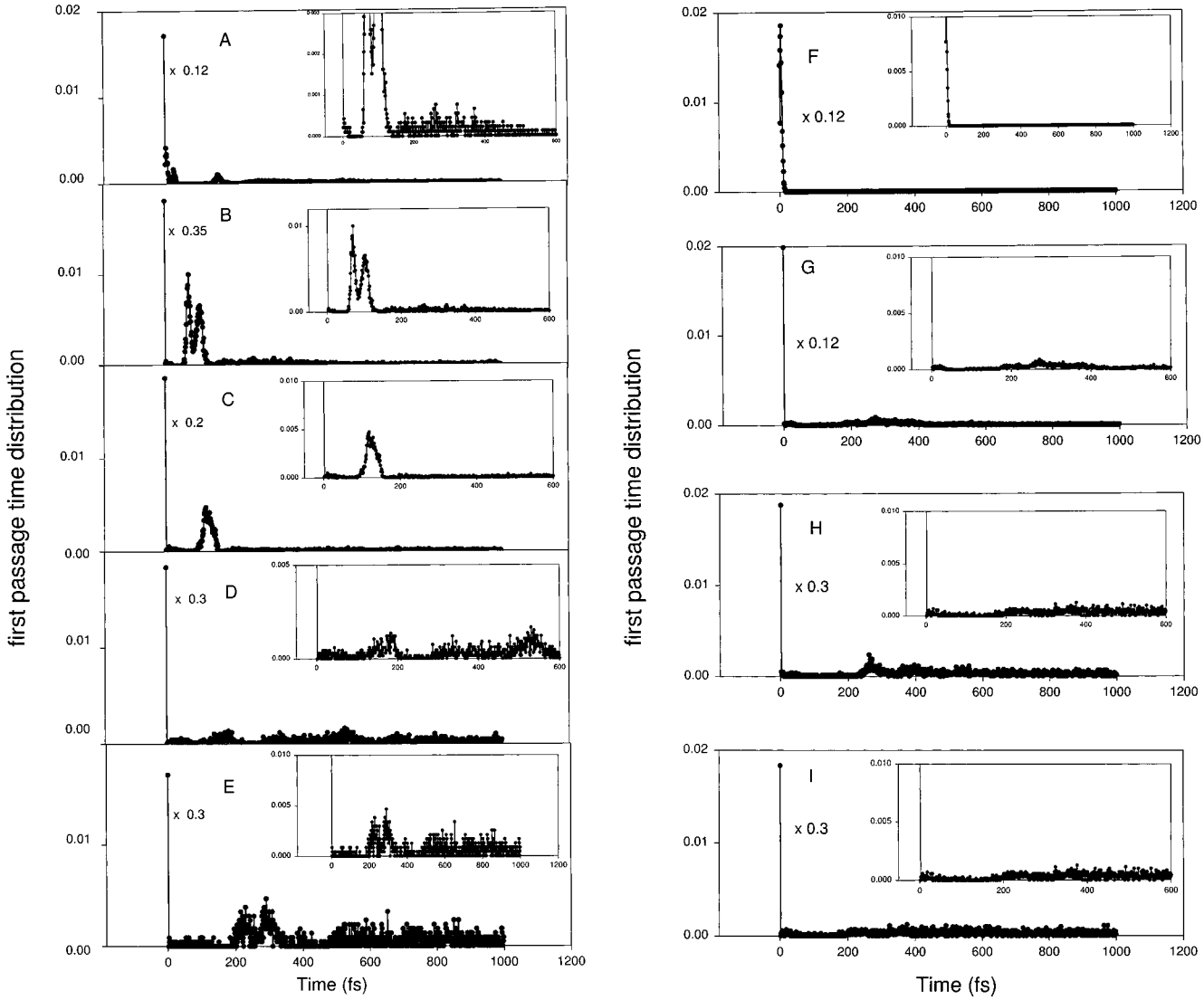

Figure 8. First passage time distribution vs time. The excitation energy is ca. 2667 K, and the local heating site is at Thr_9. The first peak (a) in (A) decreases as the site number increases. The efficiency also drops at the fourth site away from the local heating site. This shows an amino acid independent energy transfer process; i.e., the efficiency drops after an energy transfer time scale. In (F), Val_8, though next to the local heating excitation site, shows a very different distribution curve. This is due to the Mb_{20} still containing the α-helix structure. The local heating rotation follows the helix direction. This makes the O−O collision at 1 fs, and the inverse direction takes longer time to have O−O collision. Hence in the reverse direction (F) the charge transport shows different fpt distribution shape. The figures correspond to Thr_9 (A), Val_{10} (B), Leu_{11} (C), Thr_{12} (D), Ala_{13} (E), Val_8 (F), Gly_7 (G), Hsd_6 (H), and $Lysn_5$ (I).

for the vibrational energy relaxation to set in and corresponds to the cleavage of the N-terminal in the four-residue polypeptide chain experiment in ref 30.

The other way to see the higher charge transport efficiency is to examine the background temperature. One of our experimental results shows that if we excite the C-terminal with green photons (ca. 50 kcal/mol), we see no fragmentation along the chain in our $(Leu)_n$Trp experiment. The ballistic motion develops at very low background temperature. At higher background temperature, the charge transport efficiency is a product of the dynamic effect (the motion inside the BS box and the influence of phonon mode) and the electronic effect (the O−O contact distance for charge to transfer). The charge transport efficiency cannot increase once the charge is transported down along the local heating site of the polypeptide chain. We also simulated the Mb_{20} polypeptide chain with the local excitation equal to 10 000 K (i.e., 19 kcal/mol), which corresponds to 25% of the bond dissociation energy and background temperature 50 K. Because of the very weak coupling between the rotational motion and the thermal modes, the efficiency increases substantially.

The limiting case of our bifunctional model, i.e., ballistic model, admits a unit efficiency for the charge transport. Low background temperature generates a weak coupling between the phonon mode and the angular motion, which dissipates the excitation energy and lowers the efficiency. Thus, these MD calculations corroborate the experimental findings for the isolated peptide.

V. Conclusion

In summary, protein or polypeptide chains show a new distal reaction scheme. Theory now shows that the experimental observation is an essential consequence of both local excitation and a special form of protein mobility. Chemistry takes place at a long distance away from the site of original energy deposition. Such reaction rate theory is novel. Such unidirec-

TABLE 4: Efficiency at Each Site Away from the Local Heating Site[a]

residue no.	efficiency
2	0.21
3	0.0013
4	0.43
5	0.28
6	0.15
7	0.19
8	0.26
9	0.18
10	0.16
11	0.10
12	0.20
13	0.097
14	0.082
15	0.16
16	0.19
17	0.33
18	0.27
19	0.45
20	0.99

[a] Local heating site = $Lysn_{20}$. Local heating temperature = 1667 K. Background temperature = 300 K. $^{\bullet}Mb_{20}$ = (N-terminal)Glu_1-Asp_2-Leu_3-$Lysn_4$-$Lysn_5$-Hsd_6-$Gly_7-Val_8-Thr_9-Val_{10}$-$Leu_{11}-Thr_{12}$-$Ala_{13}-Leu_{14}$-$Gly_{15}-Ala_{16}-Ile_{17}$-$Leu_{18}$-$Lysn_{19}$-$Lysn_{20}$(C-terminal).

tional flow is of general importance, such as logic gates. This interesting behavior results from intrinsic properties of the charge transport process in a polypeptide. In the gas phase or in a protected environment without the solvent effect, a polypeptide chain shows a high efficiency in its charge transport behavior. Our new single site MD calculations show that our bifunctional model provides not only a dynamic explanation of the charge transport process but also presents a plausible behavior for long distance transport along a polypeptide chain. In this work, the high efficiency of the charge transport process due to the energy transfer behavior is explicitly exhibited in our bifunctional model. Our molecular single site dynamic simulation results makes it possible to pursue the motion of energy and charge down the chain and again confirms the bifunctional behavior of the charge transport process in the gas phase. The results point here to a ballistic process in the hinge motions of the protein. Such motions can have important general consequences in protein behavior. Recent results have extended this model to the liquid state and agrees with observed β values.

Acknowledgment. This work was supported by the Taiwan/Germany program at the NSC/Deutscher Akademischer Austauschdienst.

References and Notes

(1) Mayo, S. L.; Ellis, W. R., Jr.; Crutchley, R. J.; Gray, H. B. *Science* **1986**, *233*, 948.

(2) Crutchley, R. J.; Ellis, W. R., Jr.; Gray, H. B. *J. Am. Chem. Soc.* **1985**, *107*, 5002.

(3) Kostic, N. M.; Margalit, R.; Che, C−M.; Gray, H. B. *J. Am. Chem. Soc.* **1983**, *105*, 7765.

(4) Gray, H. B. *Chem. Soc. Rev.* **1986**, *15*, 17.

(5) Isied, S. S.; Kuehn, C.; Worosila, G. *J. Am. Chem. Soc.* **1984**, *106*, 1722.

(6) Nocera, D. G.; Winkler, J. R.; Yocom, K. M.; Bordignon, E.; Gray, H. B. *J. Am. Chem. Soc.* **1984**, *106*, 5145.

(7) Winkler, J. R.; Gray, H. B. *JBIC, J. Biol. Inorg. Chem.* **1997**, *2*, 399.

(8) Langen, R.; Chang, I.-Jy; Germanas, J. P.; Richards, J. H.; Winkler, J. R.; Gray, H. B. *Science* **1995**, *268*, 1733.

(9) Beratan, D. N.; Onuchic, J. N.; Betts, J. N.; Bowler, B. E.; Gray, H. B. *J. Am. Chem. Soc.* **1990**, *112*, 7915.

(10) Beratan, D. N.; Onuchic, J. N.; Winkler, J. R.; Gray, H. B. *Science* **1992**, *258*, 1740.

(11) Rajski, S. R.; Kumar, S.; Roberts, R. J.; Barton, J. K. *J. Am. Chem. Soc.* **1999**, *121*, 5615.

(12) Meggers, E.; Michel-Beyerle, M. E.; Giese, B. *J. Am. Chem. Soc.* **1998**, *120*, 12950.

(13) Jortner, J.; Bixon, M.; Langenbacher, T.; Michel-Beyerle, M. E. *Proc. Natl. Acad. Sci. U.S.A.* **1998**, *95*, 12759.

(14) Wan, C.; Fiebig, T.; Kelley, S. O.; Treaday, C. R.; Baron, J. K.; Zewail, A. H. *Proc. Natl. Acad. Sci. U.S.A.* **1999**, *96*, 6014.

(15) Isied, S. S.; Vassilian, A. *J. Am. Chem. Soc.* **1984**, *106*, 1726.

(16) Isied, S. S.; Vassilian, A. *J. Am. Chem. Soc.* **1984**, *106*, 1732.

(17) Isied, S. S.; Worosila, G.; Atherton, S. J. *J. Am. Chem. Soc.* **1982**, *104*, 7659.

(18) Mayo, S. L.; Ellis, W. R., Jr.; Crutchley, R. J.; Gray, H. B. *Science* **1986**, *233*, 948.

(19) Winkler, J. R.; Gray, H. B. *JBIC, J. Biol. Inorg. Chem.* **1997**, *2*, 399.

(20) Onuchic, N.; Beratan, D. N. *J. Chem. Phys.* **1990**, *92*, 722.

(21) Weinkauf, R.; Aicher, P.; Wesley, G.; Grotemeyer, J.; Schlag, E. W. *J. Phys. Chem.* **1994**, *98*, 8381.

(22) Weinkauf, R.; Schanen, P.; Yang, D.; Soukara, S.; Schlag, E. W. *J. Phys. Chem.* **1995**, *99*, 11255.

(23) Weinkauf, R.; Schanen, P.; Metsala, A.; Schlag, E. W.; Burgle, M.; Kessler, H. *J. Phys. Chem.* **1996**, *100*, 18567.

(24) Schlag, E. W.; Lin, S. H.; Weinkauf, R.; Rentzepis, P. M. *Proc. Natl. Acad. Sci. U.S.A.* **1998**, *95*, 1358.

(25) Baranov, L. Ya.; Schlag, E. W. *Z. Naturforsch.* **1999**, *54a*, 387.

(26) Remacle, F.; Levine, R. D.; Schlag, E. W.; Weinkauf, R. *J. Phys. Chem. A* **1999**, *103*, 10149.

(27) Schlag, E. W.; Sheu, Sheh-Yi; Yang, Dah-Yen; Selzle, H. L.; Lin, S. H. *Proc. Natl. Acad. Sci. U.S.A.* **2000**, *97*, 1068.

(28) Schlag, E. W.; Sheu, Sheh-Yi; Yang, Dah-Yen; Selzle, H. L.; Lin, S. H. *J. Phys. Chem. B* **2000**, *104*, 7790.

(29) Birks, J. B. *Photophysics of Aromatic Molecules*; Wiley: London, 1970.

(30) Schlag, E. W.; Yang, D.-Y.; Sheu, S.-Y.; Selzle, H. L.; Lin, S. H.; Rentzepis, P. M. *Proc. Natl. Acad. Sci. U.S.A.* **2000**, *97*, 9849.

(31) Berlin, Yu. A.; Burin, A. L.; Ratner, M. A. *Superlattices Microstructures* **2000**, *28*, 241.

(32) Bruinsma, R.; Grüner, G.; D'Orsogna, M. R.; Rudnik, J. *Phys. Rev. Lett.* **2000**, *20*, 4393.

(33) Brooks, B. R.; Bruccoleri, R. E.; Olafson, B. D.; States, D. J.; Swaminathan, S.; Karplus, M. CHARMM: A program for macromolecular energy, minimization, and dynamics calculations. *J. Comput. Chem.* **1983**, *4*, 187].

(34) Schanen, P. Ph.D. Thesis, Technische Universitaet Muenchen, 1997.